



Contents lists available at ScienceDirect

Arabian Journal of Chemistry

journal homepage: www.ksu.edu.sa

Original article

Anti-osteoarthritis effects of injectable hyaluronic acid hydrogel loaded with platelet lysate and cerium oxide nanoparticle by regulating TNF- α : An in vitro model

Xian Li^a, Hongkai Duan^a, Guosheng Wang^a, Mingzhang Li^a, Lifeng Zhou^a, Xin Jiang^a, Minghui Hu^a, Xiaojing Fan^a, Tao Shi^b, Fei Gao^{a,*}

^a Department of Orthopedics, Dongguan Songshan Lake Tungwah Hospital, No.1, Kefa Seven Road, Songshan Lake, Dongguan City, Guangdong Province 523808, China

^b Operating Room, Dongguan Songshan Lake Tungwah Hospital, No.1, Kefa Seven Road, Songshan Lake, Dongguan City, Guangdong Province 523808, China



ARTICLE INFO

Keywords:

Anti-osteoarthritis
CeO₂ NPs-loaded Hyaluronic Acid hydrogel
Platelet lysate

ABSTRACT

The most prevalent type of joint illness is osteoarthritis, also known as OA. The inflammation of the joint is strongly linked to both the beginning and the progression of osteoarthritis. The use of hydrogels as an OA treatment has the potential to go beyond the administration of anti-inflammatory components to have an inherent immunomodulatory role. Platelet lysate (PL) contains a cocktail of growth factors that actively participates in cartilage repair. Moreover, cerium oxide-nanoparticles (CeO₂-NPs) have been broadly studied owing to their powerful antioxidant properties and potential preventive and therapeutic effects against chronic diseases. The current study was designed to determine the effect and mechanism of injectable hyaluronic acid (HA) hydrogel loaded with PL and CeO₂-NPs on OA. The results showed that the obtained PL and synthesized CeO₂-NPs were effectively incorporated into HA hydrogel and the resultant hydrogel was injectable and have a porous micro structure with interconnected pores. The biological evaluation by qPCR revealed that the fabricated hydrogel exhibited a significantly increased expression of Col2 and Aggrecan (TNF- α -suppressed anabolic molecules) and decreased expression of Col10, Mmp13, Adamts5, and Adamts9 (TNF- α -activated catabolic molecules). Also, ELISA results confirmed this potent antioxidant activity of hydrogel and also increased the growth of chondrocytes over the culturing period.

1. Introduction

The most common form of chronic joint illness, osteoarthritis, is linked to alterations at molecular, biochemical, morphological, and biomechanical levels in all components of the affected joint. It is characterized by the progressive degradation of articular cartilage and abnormal bone remodeling. Several factors contribute to the onset of osteoarthritis, with aging being the most significant. These factors encompass gender, obesity, genetic predisposition, mechanical stress, and others. (Abramoff and Caldera, 2020; Wieland et al., 2005; Zhang and Jordan, 2010). An important aspect of the aging process is the development of systemic inflammation. Inflammatory cytokines trigger the secretion of matrix metalloproteinases (MMPs) and a disintegrin and metalloproteinase with thrombospondin motifs (ADAMTs) by chondrocytes and synoviocytes. These enzymes contribute to the breakdown

of the cartilage matrix. Mechanical overloading can directly stimulate the release of inflammatory cytokines by chondrocytes and indirectly lead to synovial inflammation by generating cartilage fragments. This process results in an increase in inflammatory cytokines in the synovial fluid, ultimately impacting joint health negatively. Additionally, the redox status substantially influences chondrocyte function. (Hamerman, 1989; Goldring and Otero, 2011; Scanzello and Goldring, 2012).

ROS and RNS are abbreviations that stand for "reactive oxygen species" and "reactive nitrogen species," respectively. These terms refer to reactive free radicals and non-free radical derivatives of oxygen and nitrogen, respectively, which are the primary variables that control the redox homeostasis in cells (Chen et al., 2020). During cellular senescence, the activity of antioxidant enzymes such as superoxide dismutase (SOD) and glutathione peroxidase (GSH) decreases, while systemic inflammation and mitochondrial failure, hallmarks of senescence,

Peer review under responsibility of King Saud University.

* Corresponding author.

E-mail address: goldfei78@163.com (F. Gao).

<https://doi.org/10.1016/j.arabjc.2023.105488>

Received 22 July 2023; Accepted 26 November 2023

Available online 28 November 2023

1878-5352/© 2023 The Authors. Published by Elsevier B.V. on behalf of King Saud University. This is an open access article under the CC BY-NC-ND license (<http://creativecommons.org/licenses/by-nc-nd/4.0/>).

contribute to increased formation of reactive oxygen species (ROS) and reactive nitrogen species (RNS). Oxidative stress results from an imbalance in the production of ROS/RNS and the scavenging action of the antioxidant system. (Qiu et al., 2018; Wang et al., 2017). Damage to DNA, protein peroxidation, and lipid peroxidation can all be brought on by oxidative stress. Damage to the mitochondria's DNA, in turn, makes the mitochondrial malfunction even worse. ROS and RNS both contribute to the generation of inflammatory cytokines by activating the NF- κ B pathway through the modification of IB kinase. Lipid peroxides, such as ox-LDL, are another factor that contribute to the development of systemic inflammation (Lu et al., 2021; Coryell et al., 2021; Rhoads and Major, 2018). According to Bai et al. 2019, ROS and RNS both hinder the formation of cartilage matrix through regulating the PI3K/Akt and MAPK pathways, and increase the breakdown of cartilage matrix either directly or indirectly by boosting the expression of matrix metalloproteinases (MMPs) (Bai et al., 2019).

The majority of pharmacologic treatments for osteoarthritis (OA), such as nonsteroidal anti-inflammatory drugs and intraarticular injections of glucocorticoids, primarily aim to alleviate symptoms. However, none of these treatments have been proven to halt the progression of the disease or reverse cartilage degradation in patients. In cases where patients do not benefit from more conservative treatment options, surgery may be considered as a management alternative, albeit as a last resort. Meanwhile, a wide range of potential complications associated with surgery, such as infections, thrombosis, and nerve and vascular damage, can pose an increased risk of mortality in elderly patients. (Lin et al., 2020; Hawker and King, 2022; Sperati et al., 2008).

The administration of hyaluronic acid (HA) via intra-articular injection, a medical intervention first approved for use in the United States by the Food and Drug Administration in 1999, has recently gained traction as one of the most popular non-surgical therapy options for alleviating symptoms of OA. HA, a vital component of healthy synovial fluid, plays a crucial role in enhancing the viscosity of the synovial fluid and acts as a shock absorber to shield soft tissues from damage. Moreover, HA facilitates smoother joint movement by forming a protective layer on the cartilage, provides relief from discomfort, and significantly contributes to joint homeostasis due to its immunomodulatory effects on inflammatory cells. It has the potential to reduce the production of pro-inflammatory mediators and the activity of MMPs. HA can also serve as the foundation for various scaffolds, carriers, and structures used in drug delivery and regenerative medicine when combined with nanotechnology, cell therapy, and traditional medicine. (Chen et al., 2020; Wang et al., 2023; Li et al., 2023; Su et al., 2022).

Metal/metal oxide NPs (~100 nm) exhibit distinct physical characteristics compared to microparticles (500 nm ~). The high surface reactivity of NPs is due to the fact that they have a large surface area relative to their volume (Ejaz et al., 2023; Khan et al., 2023). These outstanding properties have made them promising structures for various applications (Imran et al., 2023; Muzaffar et al., 2023; Afzal et al., 2023; Huang et al., 2023). On one hand, this allows them to mimic the functioning of various antioxidant enzymes, such as SOD and catalase (CAT). Broadly speaking, smaller particle sizes result in stronger catalytic activity. On the other hand, it allows them to readily adhere to cell membranes, thereby enhancing cellular absorption. Through the regulation of the redox state and the release of metal ions, metal and metal oxide NPs can exert anti-oxidative stress, radical scavenging, and anti-inflammatory effects upon entering cells. (Wang et al., 2023; Agarwal et al., 2019).

In a redox reaction, cerium oxide (CeO₂) may coexist in both the trivalent (+3) and tetravalent (+4) states; as a result of its significant redox capacity, it is believed to be an effective free radical scavenger. Changes in this oxidation state are dynamic, and they are brought about by either oxygen vacancies or oxygen deficits in the lattice structure (Esch et al., 2005). They can happen on their own or in reaction to varied physiological conditions or physical characteristics. This is due to the fact that smaller organisms generate more oxygen vacancies than larger

organisms do. In this redox process, size is one of the most important criteria to consider. According to this evidence, CeO₂-NPs have the potential to become an effective antioxidant agent (Nelson et al., 2016; Karakoti et al., 2008). In point of fact, CeO₂-NPs have been investigated for their usage as possible therapeutic agents in a variety of diseases and disorders caused by oxidative stress, including Alzheimer's disease (Reed et al., 2014; Celardo et al., 2011; Walkey et al., 2015; Kwon et al., 2016). In the current study, CeO₂-NPs were introduced into the injectable HA hydrogel and we believe that cerium oxide is capable of shielding HA from degradation, and CeO₂ NPs-loaded injectable HA hydrogel can prevent oxidative stress caused by hydrogen peroxide on chondrocytes.

2. Materials and methods

2.1. Materials

Cerium (III) nitrate hexahydrate (Ce (NO₃)₃·6H₂O, Hyaluronic acid sodium salt (HA; Mw 1.3 × 10⁶ Da), 1, 4-butanediol diglycidyl ether (BDDE), potassium carbonate, and NaOH were obtained from Sigma-Aldrich (St. Louis, MO, USA).

2.2. Synthesis and characterization of CeO₂-NPs

The CeO₂-NPs were synthesized based on previous reports with minor modification. Briefly, 1.085 g, Ce (NO₃)₃·6H₂O was dissolved in 125 mL double distilled water to obtain a 0.02 M solution. Simultaneously, 518 mg K₂CO₃ was dissolved in 250 mL double distilled water to obtain 0.03 M solution. Then, 50 mL of the cerium solution was added dropwise to 20 mL of potassium carbonate under vigorous stirring. The pH of the reaction mixture was set at 6.0 during the synthesis. The aging process was conducted at 220 °C for 150 min without any further washing steps. Finally, the aged NPs were calcined at 600 °C for 180 min. The synthesized CeO₂-NPs were characterized using Scanning electron microscopy (SEM, JSM-7600F. JEOL, Tokyo, Japan) at the accelerating voltage of 20 kV. CeO₂-NPs were mounted on the adhesive copper stub and sputter-coated with electroconductive element (gold). Using TEM instrument (ZEISS CEM 902 A) the morphology of CeO₂-NPs were evaluated. A small droplet of NPs dispersion was dried on a TEM grid and visualized at a voltage of 200 kV. The hydrodynamic size and Zeta potential of the synthesized CeO₂-NPs were investigated using a Zeta-sizer Nano ZS (Malvern Instruments Ltd, UK) at 25 °C. Using a Thermo Scientific Genesys 6 UV-Vis spectrophotometer the UV-Vis spectra of the synthesized CeO₂-NPs was recorded. The analysis was conducted using quartz cuvettes of 1 cm in length in the range of wavelengths between 200 and 900 nm. The FTIR spectra of the synthesized CeO₂-NPs was obtained using a VERTEX 70 V (Bruker, Germany) spectrometer at room temperature over the wavenumber range of 4000—400 cm⁻¹. Using the DPPH (1, 1-diphenyl-2-picrylhydrazyl) assay kit the radical scavenging potential of the synthesized CeO₂-NPs was evaluated. According to the previous report (Soren et al., 2015), different concentrations of CeO₂-NPs (10, 20, 40, 100, 200 µg/mL) were dispersed in one mL of methanol and incubated with a reaction mixture contained DPPH (76 µM). The reaction mixture was allowed to incubate for 60 min at room temperature, and the absorption was measured at 517 nm using a microplate reader.

2.3. Platelet lysate preparation

Platelet lysate (PL) was obtained from rat plasma platelet concentrates following a two-step procedure, adapted from previous studies. In this modified method, the anti-coagulated blood (in 3 % v/v sodium citrate) underwent a 10-minute centrifugation at 210 × g at 4 °C to yield a yellowish fraction containing plasma with buffy coat, which was further centrifuged at 4 °C for 5 min at 210 × g. Subsequently, a series of three freeze-thaw cycles between -80 °C and 37 °C resulted in the lysis

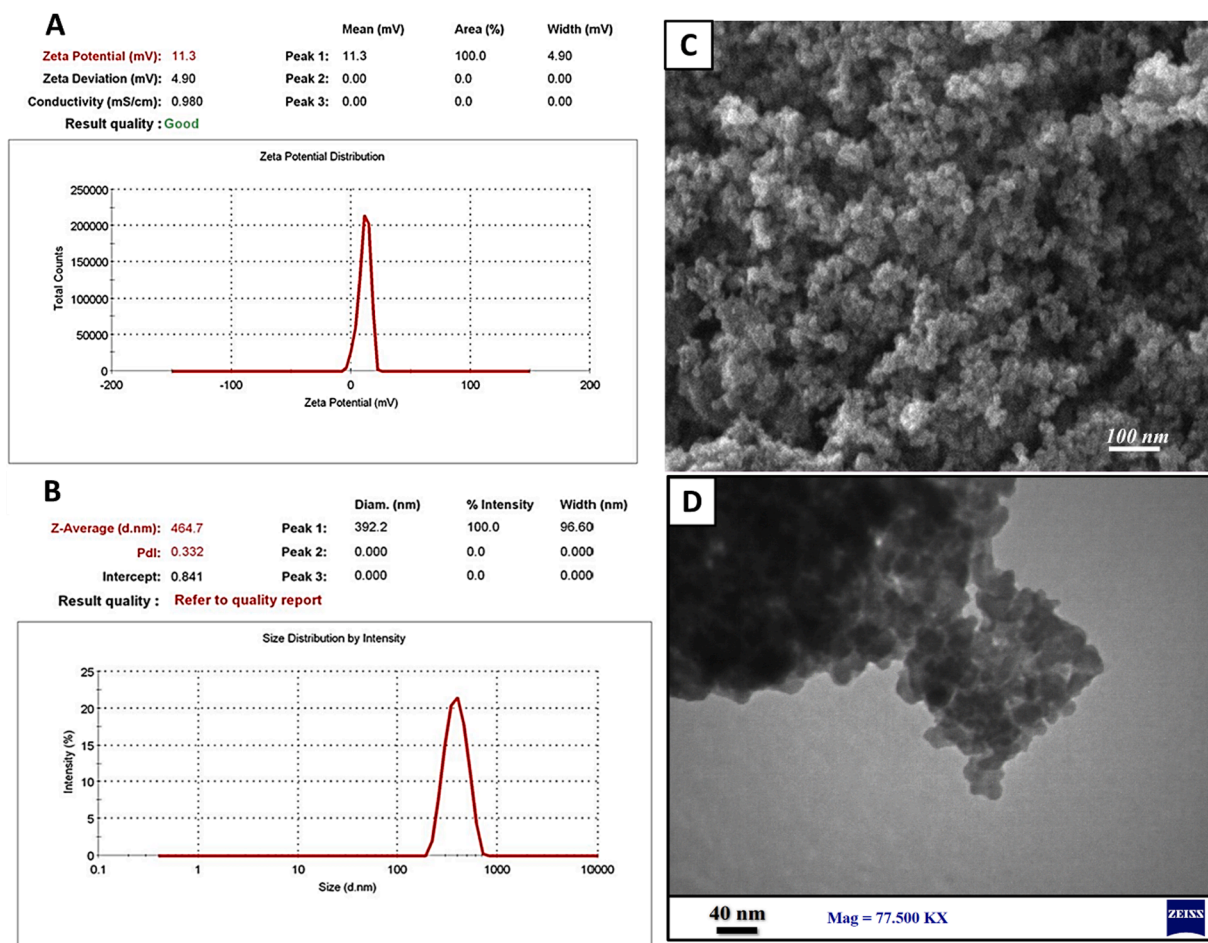


Fig. 1. Characteristics of CeO₂-NPs. (A) Zetapotential, (B) hydrodynamic size, (C) SEM image, and (D) TEM image of CeO₂-NPs.

of concentrated platelets, and the remaining platelet residue was then removed by centrifugation at 2,000 × g for 10 min.

2.4. Fabrication of injectable hyaluronic acid hydrogel

The hydrogel was prepared using a solution impregnation based on previous protocol with minor revision. For pure hydrogel synthesis, HA was dissolved in 0.1 M NaOH solution and stirred for 24 h at room temperature to obtain a homogenous solution of 2 % (w/v) HA. The obtained polymeric solution was blended with BDDE solution (1 % w/v) containing 0.1 M NaOH and gently shaken for one h and incubated at 30 °C for 12 h to complete the cross-linking. The hydrogel was rinsed with ultra-pure water three times to eliminate any unreacted residual substances. We followed a similar protocol to produce the HA hydrogel loaded with PA and CeO₂ NPs, with the exception of the initial step. In this case, we introduced CeO₂ NPs (5 % w/v) and PL (5 %w/v) into the starting solution, after which we added HA and proceeded with the aforementioned protocol.

2.5. Characterization of hydrogel

The hydrogels' morphology was examined using the SEM imaging technique. Following lyophilization with a freeze-dryer (Thermo Heto PowerDry LL3000, USA), the hydrogels were cross-sectioned with a thin blade, coated with gold, and then observed using an SEM microscope. Furthermore, the semi-quantitative elemental analysis and distribution of CeO₂ nanoparticles within the hydrogel were assessed using EDX analysis. This experiment was performed using the SEM apparatus integrated with an EDX detector following gold coating. The surface

functional groups of the synthesized CeO₂ NPs and the fabricated nanocomposites was evaluated using the FTIR spectroscopy (VERTEX 70 V spectrometer, Bruker, Germany) at room temperature over the wavenumber range of 4000—400 cm⁻¹. The XRD pattern of the fabricated hydrogels was obtained using a PANalytical Empyrean diffractometer (PANalytical, USA). The experiment was conducted on lyophilized samples after pressing them into flat samples and mounting them onto a quartz sample holder. The using a Cu K α radiation (45 kV and 40 mA) and a step size of 0.026°. The injectability of the prepared hydrogel was assessed by examining its ability to be loaded into a syringe. The flow of the hydrogel from the syringe under a constant piston pressure served as an indication of its injectability. To evaluate the water absorption capacity of the hydrogels, they were immersed in PBS and the resulting weight change was measured. The hydrogel samples were then freeze-dried, weighed, immersed into a solution, incubated for 48 h, and their wet weights were measured at preselected times. The obtained values were used to calculate the water absorption percentage for the formulation.

$$\text{Water absorption (\%)} = \left(\frac{\text{wetweight} - \text{initialdryweight}}{\text{initialdryweight}} \right) \times 100$$

2.6. Biological evaluations

The cytocompatibility of the fabricated hydrogels was assessed using the MTT assay kit. The samples in their wet form underwent sterilization through 20 min of UV irradiation, followed by a 20-minute incubation in 70 % ethanol and three washes with autoclaved PBS (pH: 7.4). Subsequently, the sterilized hydrogels were incubated with 10⁵ cells per well

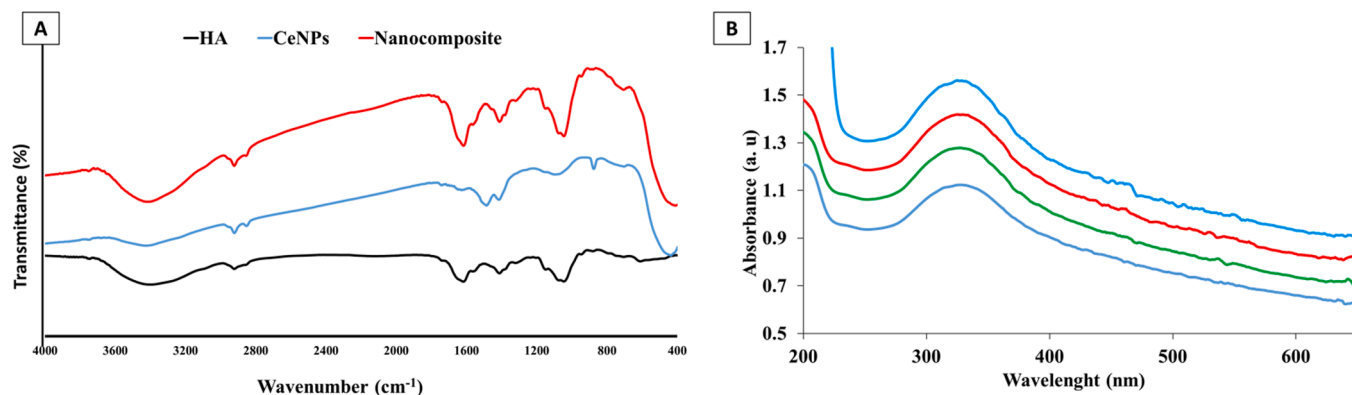


Fig. 2. FTIR spectrum (A) and UV-Vis spectrum (B) of CeO₂-NPs.

in 96-well plates, each containing 100 μ l of cell culture medium (DMEM)/FBS (10 %)/Pen-Strep. The cells were then incubated for 48 and 72 h under standard cell culture conditions. For the 72-hour incubation group, the cell culture medium was refreshed once. At the end of the designated incubation period, MTT solution was added to the cells and incubated for 4 h in the dark. Following this, a DMSO solution was added to the cells, and the absorbance of the medium was measured at 590 nm using a microplate reader. Wells without hydrogels served as the control group. The percentage of cell viability was calculated using the following equation:

$$\text{Cellviability}(\%) = \left(\frac{OD_{\text{test}} - OD_{\text{Background}}}{OD_{\text{control}} - OD_{\text{Background}}} \right) \times 100$$

Real time PCR (qPCR) assay was applied to evaluate the expression of target genes under treatment. The cells were treated with TNF- α (10 ng/ml) for 6 h to induce OA. The cells without any treatments were considered as healthy cells, the cells treated with only TNF- α as the control group, and the cells treated with TNF- α plus hydrogel as the treatment. TRizol reagent was applied to extract total RNA and the quality of the product was evaluated by NanoDrop2000 spectrophotometer. Then, cDNA was synthesized by the reverse transcription. The applied reaction mixture (20 μ l) comprising PCR Forward Primer (0.4 μ l), template cDNA (1 μ l), SYBR® Premix Ex Taq II (Tli RnaseH Plus) (10 μ l), PCR Reverse Primer (0.4 μ l) and ddH₂O (8.2 μ l). The qPCR reaction was conducted using the following condition: initial denaturation at

95 $^{\circ}$ C for 5 min, denaturation at 95 $^{\circ}$ C for 10 sec (40 cycles), and annealing and extension at 60 $^{\circ}$ C for 30 sec. The reference gene was β -Actin and the relative mRNA expression was measured using the $2^{-\Delta\Delta CT}$ method. The experiment was conducted using an ABI QuantStudio™ 7 Flex Real-Time PCR System.

Concentrations of *Col2*, *Aggrecan*, *Col10*, *Mmp13* (Cloud Clone, USA) and *Adams1*, *Adams9* (MyBioSource, USA) in the cell culture supernatant were determined using commercially available ELISA kits according to the instructions provided by the manufacturer. A standard curve was calculated for each assay with detection limits based on protocol assay. Values are presented in ng/mL.

2.7. Data analysis

Using the statistical analyzing software (SPSS, 16.0, SPSS Inc., Chicago, IL, USA) the obtained data (carried out at least in triplicate) were analyzed and expressed as mean \pm SD. The p-value less than 0.05. was considered as statistically significance of the results.

3. Results and discussion

3.1. CeO₂-NPs properties

The hydrodynamic and actual size, surface zeta potential, and morphology of the synthesized CeO₂-NPs were characterized using DLS,

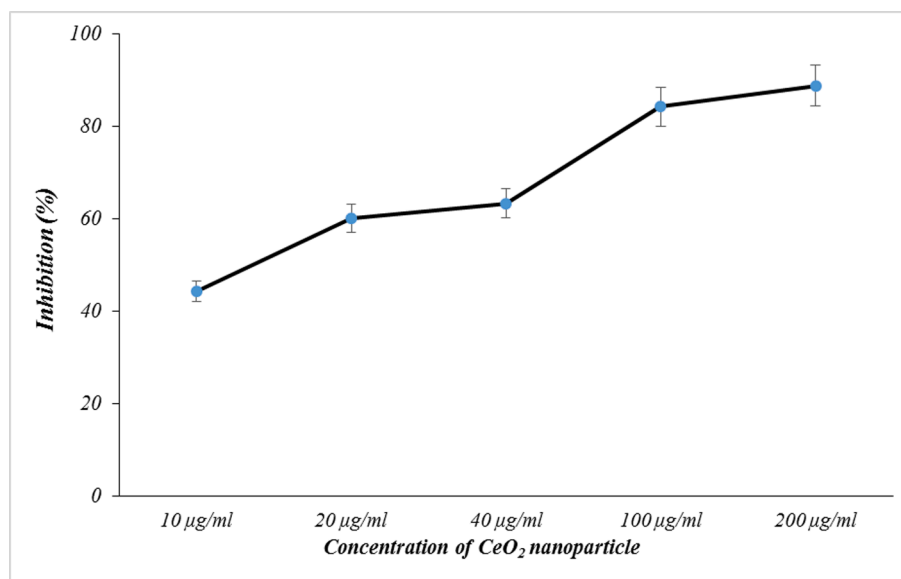


Fig. 3. Radical scavenging activity of CeO₂-NPs, measured using the DPPH assay kit.

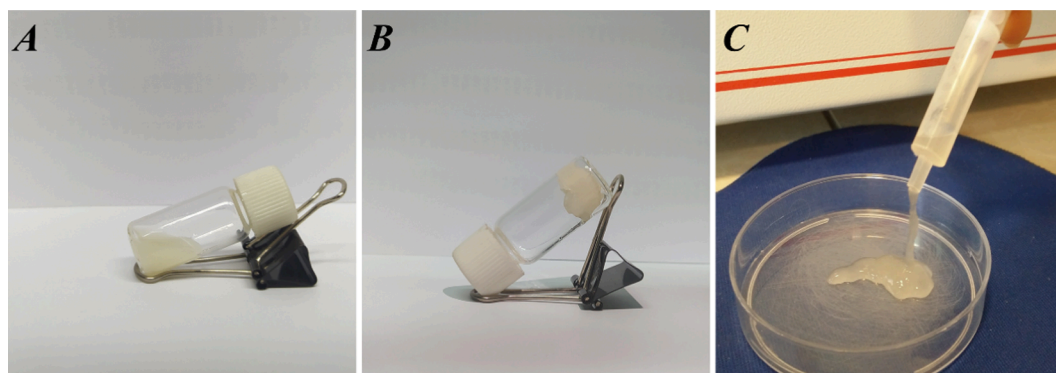


Fig. 4. Macroscopic features of the hydrogel. (A) Polymeric solution, (B) the formed hydrogel, and (C) syringeability of the hydrogel.

Zetasizer, and SEM/TEM imaging, respectively. The results revealed that the synthesized CeO₂-NPs have a zeta potential of 11 ± 2 mV (Fig. 1A) and a hydrodynamic size of 460 ± 20 nm (Fig. 1B). The morphology of the synthesized CeO₂ NPs was observed through SEM (Fig. 1C) and TEM (Fig. 1D) imaging, showing a spherical and uniform morphology. These findings are consistent with those reported in other studies.. Lin et al. (Lin, 2020) synthesized nanoceria and observed cubic crystals CeO₂-NPs agglomerates under SEM imaging. They reported a

hydrodynamic size of 131 ± 0.7 nm with the PDI value of 0.104. In another study, Marzi et al. (De Marzi et al., 2013) synthesized ceria NPs observed spherical agglomerates of NPs under SEM imaging. Tumkur et al. (Tumkur et al., 2021) used a hydroxide-mediated method to synthesize cerium oxide nanoparticles and observed clusters of uniformly distributed particles through SEM imaging.

The FTIR spectroscopy was conducted to evaluate the functional groups of the synthesized CeO₂-NPs and the results are presented in

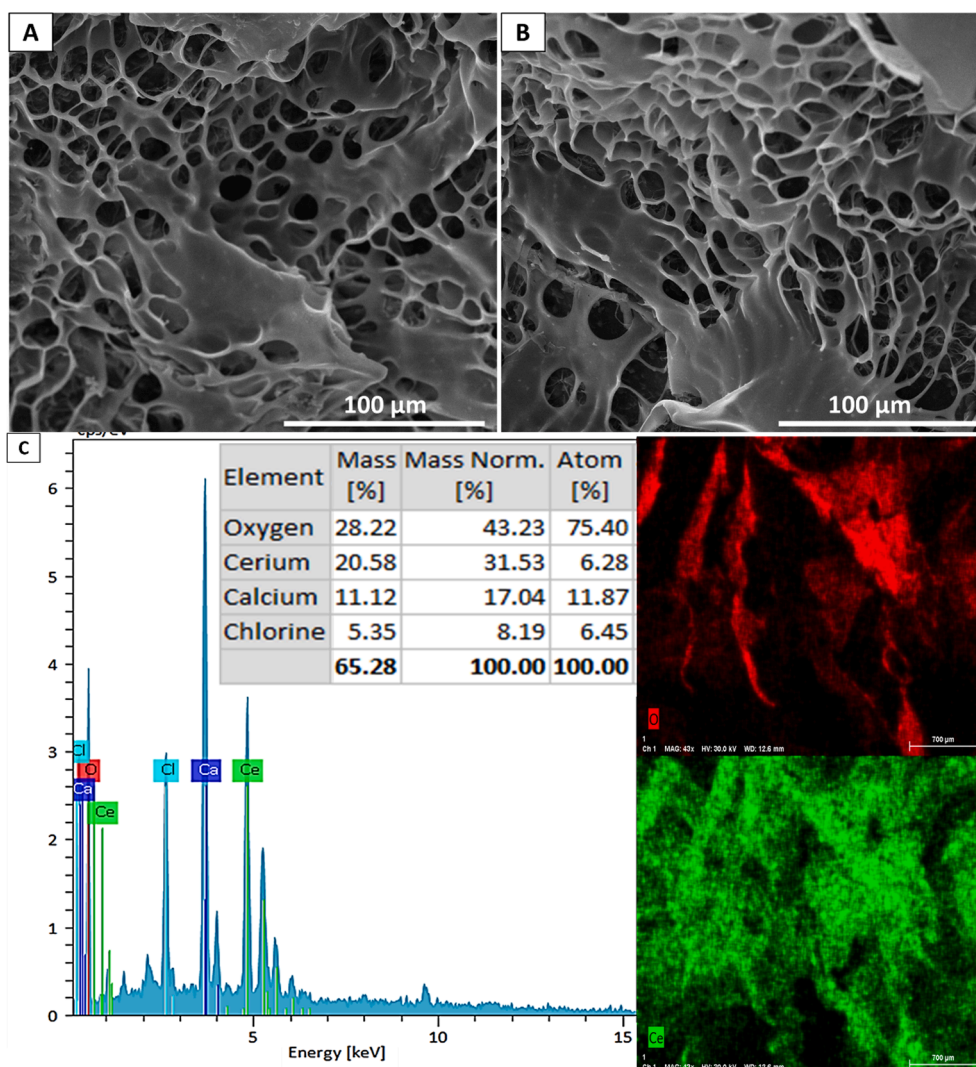


Fig. 5. SEM image of (A) pure HA hydrogel, (B) CeO₂ NPs-loaded hydrogel, and (C) EDX analysis results.

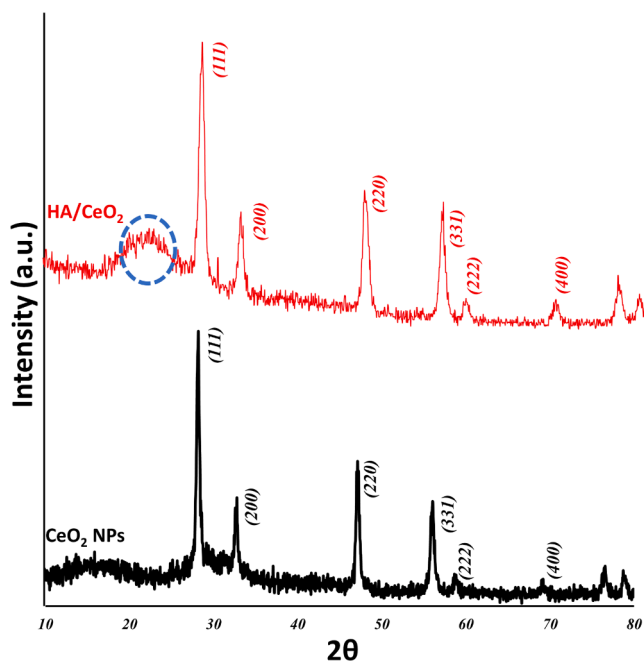


Fig. 6. XRD patterns of the synthesized CeO₂-NPs and HA/CeO₂-NPs hydrogel.

Fig. 2A. The characteristic peaks of HA can be seen around 1600 cm^{-1} (related to antisymmetric stretching vibration of COO^-), 1405 cm^{-1} (related to symmetric stretching vibration of COO^-), 3427 cm^{-1} (related to the plethora of hydroxyl groups, O–H stretching), and 2922 cm^{-1} (related to the aliphatic symmetric C–H group stretching) (Culica et al., 2020; Safat et al., 2021). In the FTIR spectrum of the synthesized CeO₂-NPs the peak located at around 3420 cm^{-1} can be attributed to the –OH stretching vibrations of the hydroxyl groups. Moreover, the peaks related to the –CH₃ and –CH₂ asymmetric stretching vibrations can be seen at around 2850 cm^{-1} and 2920 cm^{-1} . The peak located at around 450 cm^{-1} can be attributed to CeO₂ stretching vibration (Zamiri et al., 2015). The FTIR spectrum of the hydrogel nanocomposite exhibited the characteristic peaks of HA, indicating the entrapment of CeO₂-NPs into the hydrogel.

The UV–Vis spectrum of the synthesized CeO₂-NPs was recorded and the results are presented in Fig. 2B. The characteristic absorption peak of Ce⁺⁴ and Ce⁺³ of CeO₂-NPs can be seen around 325 and 200 nm.

According to the results, it can be concluded that the synthesized CeO₂-NPs consist of Ce⁺⁴ and Ce⁺³ ions. It is reported that the presence of Ce⁺³ ions has direct and vital roles in radical scavenging activity of CeO₂-NPs (Dunnick et al., 2015; Nurhasanah et al., 2018).

The antioxidant activity of the synthesized CeO₂-NPs was assessed using the DPPH assay kit. DPPH is a stable free radical and antioxidant substance that neutralizes this free radical via donation of hydrogen or electron and forms the stable DPPH molecule (Nurhasanah, 2018). The results of the experiment revealed a dose-dependent radical scavenging activity of the synthesized CeO₂-NPs (Fig. 3).

3.2. Hydrogel nanocomposite properties

The hydrogel was created through the interaction of BDDE with HA polymer, which led to the formation of covalent ether linkages between adjacent HA-HA polymeric chains. Furthermore, the interconnected HA-HA network structure and the abundant surface OH groups are believed to facilitate macromolecular entanglements and hydrogen bonding. The transformation from sol to gel and the injectability of the resulting hydrogel are illustrated in Fig. 4A–D. The results (Fig. 4C) demonstrate the consistent flow of the hydrogel through the syringe.

3.3. SEM and EDX results

In addition to macroscopic characteristics, microscopic properties such as internal structure, porosity, and pore architecture are essential and decisive for the intended application. We utilized SEM imaging to examine the internal structure and pore architecture of pure and CeO₂-NPs-loaded hydrogels, and the findings are depicted in Fig. 5. It is evident that the fabricated hydrogels possess a porous structure with interconnected pores. Furthermore, the incorporation of CeO₂-NPs into the HA hydrogel (Fig. 5B) did not alter the structure of the HA hydrogel (Fig. 5A). Numerous studies have underscored the use of porous hydrogels for osteoarthritis treatment. (Zhao et al., 2022). The porous nature of the hydrogels can be applied to deliver various therapeutic agents. It was observed that porous hydrogels can provide slow and sustained release of the therapeutic agents into the synovial cavity and subsequently, effectively promote cell proliferation, tissue formation, and repairing cartilage (Jeuken et al., 2016; Réeff et al., 2013). The distribution of CeO₂-NPs within the HA hydrogel was evaluated using the semi-quantitative EDX analysis. The results (Fig. 5C) showed that the synthesized CeO₂-NPs are homogeneously dispersed within the matrix of the HA hydrogel.

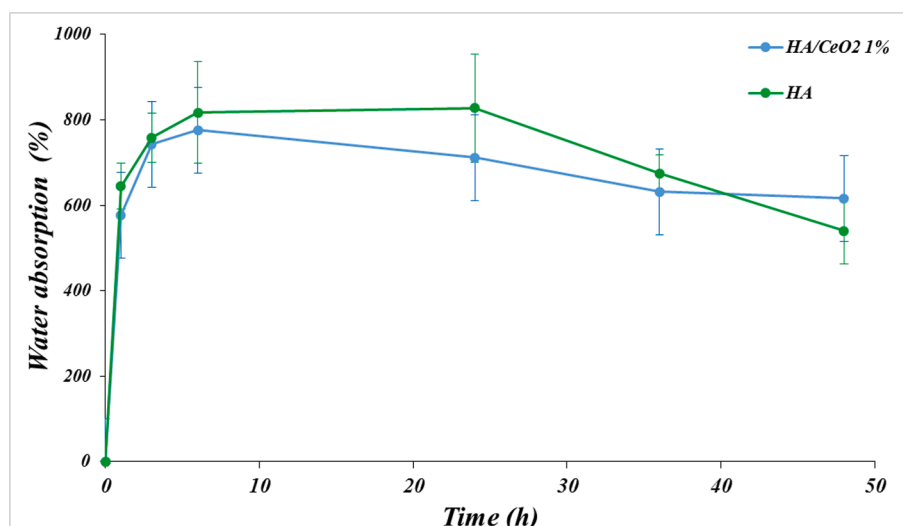


Fig. 7. Water absorption and retention of the fabricated hydrogels.

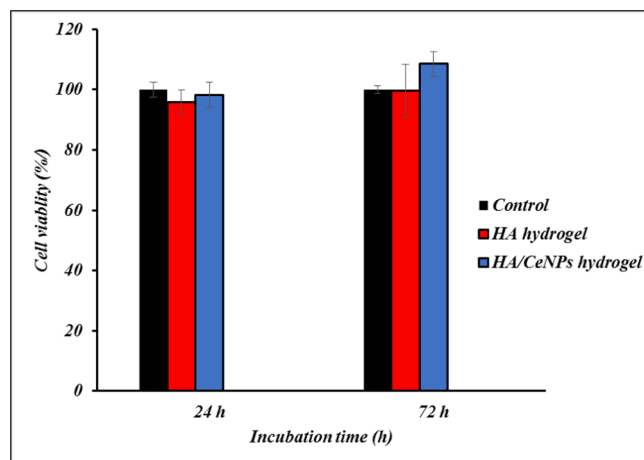


Fig. 8. Cell viability results of the fabricated hydrogels at 24 and 72 h after cell seeding, measured by the MTT assay.

3.4. XRD results

The crystallinity of the synthesized CeO₂-NPs and fabricated hydrogel was evaluated using the XRD analysis. The XRD pattern of CeO₂-NPs (Fig. 6) showed that the CeO₂-NPs exhibited the characteristic peaks of CeO₂ NPs. The peaks and indicating lattice planes are as follow: $2\theta = 28.5^\circ$: (1 1 1), $2\theta = 33.9^\circ$: (200), $2\theta = 47.8^\circ$: (220), $2\theta = 56.2^\circ$: (3 1 1), $2\theta = 58.5^\circ$: (222), and $2\theta = 69.1^\circ$: (400). The obtained XRD pattern is match with JCPDS No. 340,394 (standard cerium oxide pattern) (Lin, 2020; Kumar et al., 2010; Farahmandjou et al., 2016). Moreover, the wide peak at the HA/CeO₂-NPs pattern located at 22° to 25° can be associated to the reflection at (1 1 0) and (200) diffraction planes of HA structure (Fig. 6), indicating the semi-crystalline nature of fabricated HA hydrogel (Sundarrajan et al., 2012; Hezma et al., 2023). In this pattern (HA/CeO₂-NPs) the characteristic peaks of CeO₂-NPs can be observed, indicating that the incorporation of CeO₂-NPs into the hydrogel structure did not alter the crystallinity of the synthesized CeO₂-NPs. Moreover, using the Debye-Scherrer equation we found that the synthesized NPs have an average crystallite size (D) of around 8 nm.

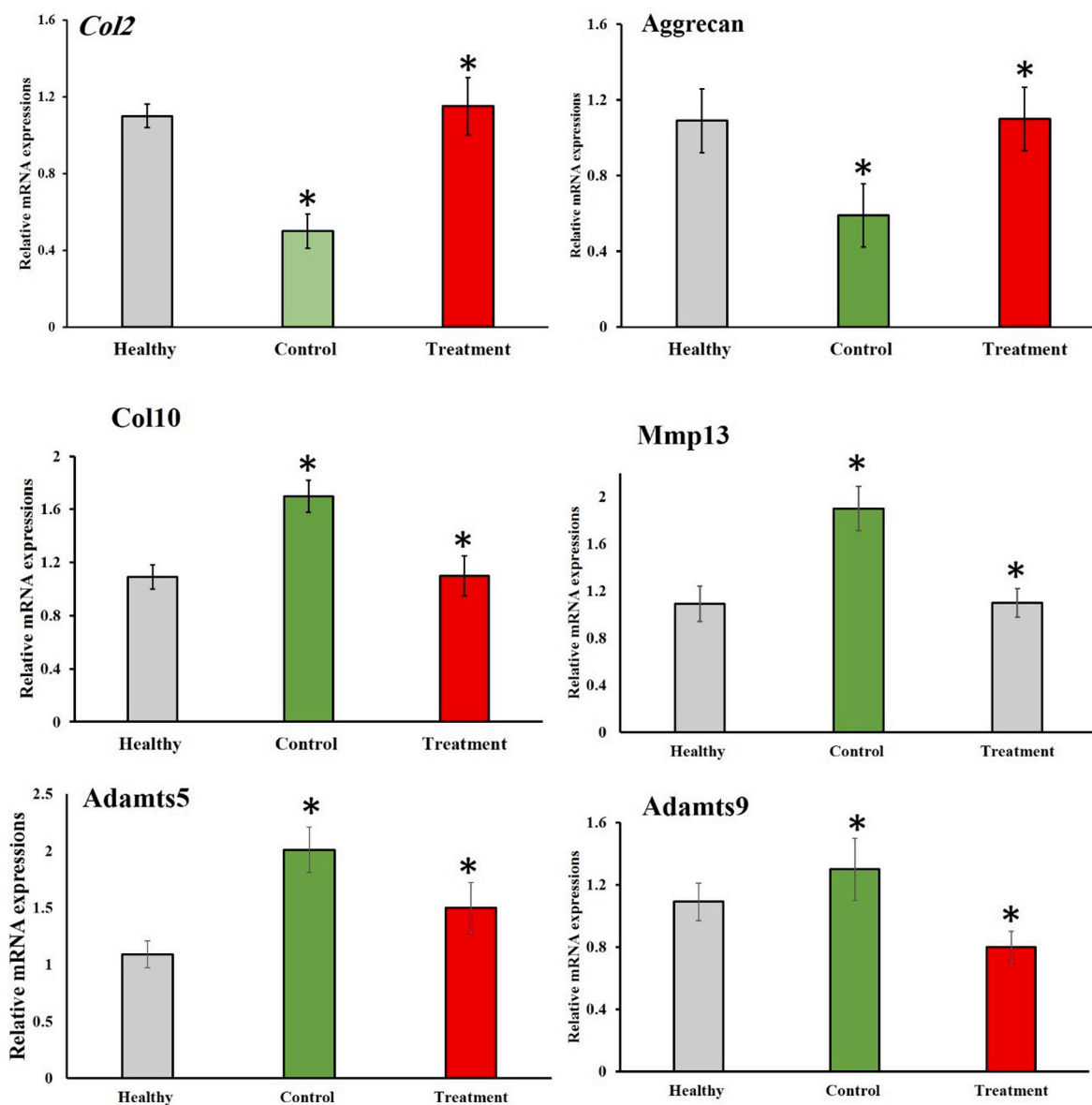


Fig. 9. Relative mRNA expressions of Col2, Aggrecan, Col10, Mmp13, Adamts, Adamts9 genes in chondrocytes treated with TNF- α (Control) and TNF- α plus hydrogel. Values are shown as mean \pm SD. *P < 0.05.

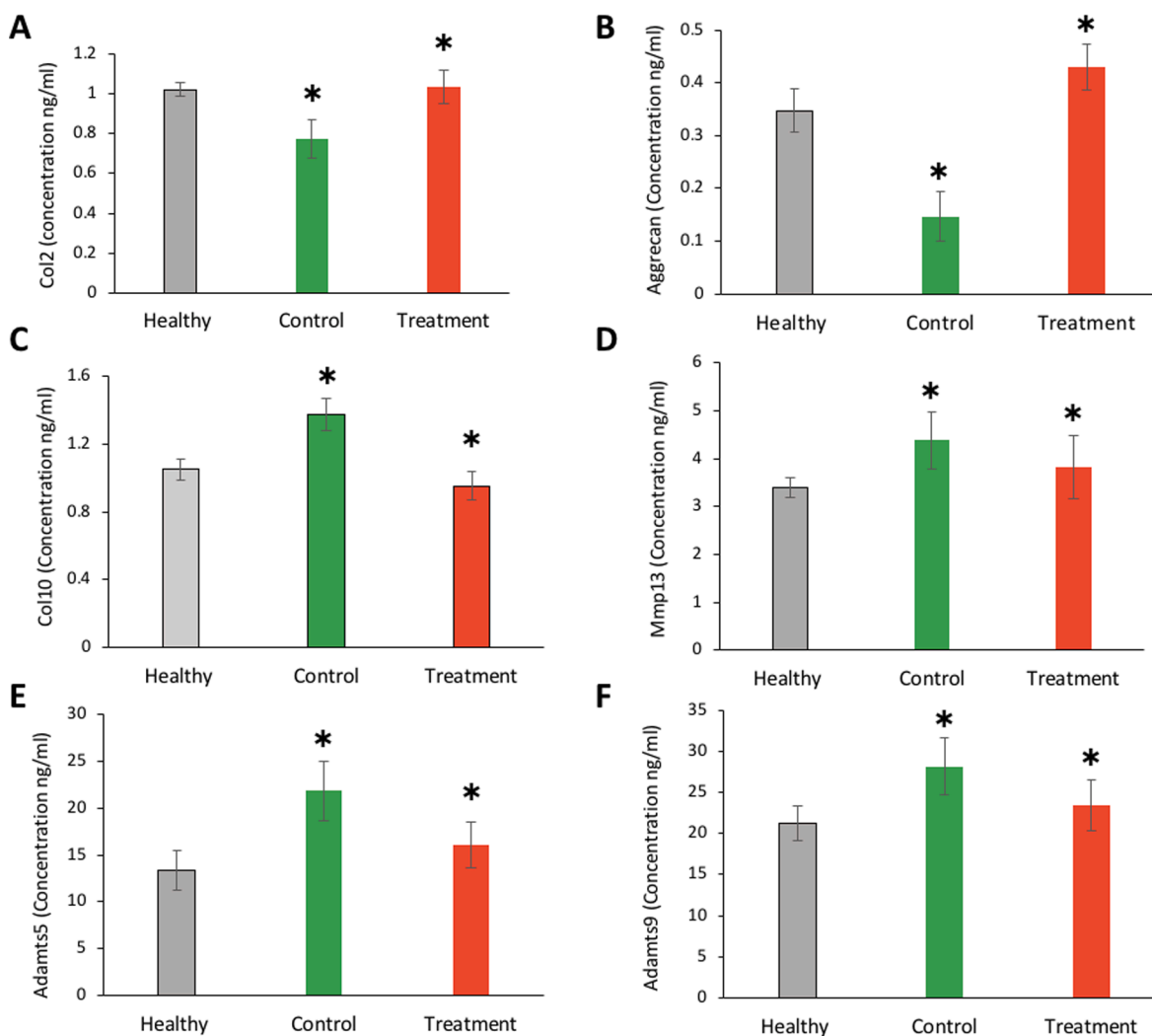


Fig. 10. Concentration (ng/ml) of Col2, Aggrecan, Col10, Mmp13, Adams5, Adams9 in the cell culture treated with TNF- α (Control) and TNF- α plus hydrogel. Values are shown as mean \pm SD. *P < 0.05.

$$D = \frac{k\lambda}{\beta \cos \theta}$$

3.5. Swelling results

The water absorption capacity and water content are essential indicators for biomaterials, especially in the context of osteoarthritis treatment. Hydrogels with high water absorption and retention capacity have garnered significant attention for their potential to alleviate symptoms of OA. We conducted an assessment of the water absorption and retention capacity of the prepared hydrogels, and the results (Fig. 7) indicate that the fabricated hydrogels swelled by 800 % within the initial 10 h of the experiment. Furthermore, the hydrogels retained the absorbed water for approximately 25 h before the retention decreased. These findings suggest that the structure of the hydrogel remains stable and intact within the first 24 h, after which the cross-linking of the biopolymer is broken down through hydrolysis, leading to desorption. Additionally, we observed that the inclusion of CeO₂-NPs in the HA hydrogel reduced its water absorption and retention potential. This observation may be attributed to interactions between the NPs and the hydrophilic groups of the HA polymer, which occupied these groups and hindered the absorption of water through these functional groups. Zhang et al. (Zhang et al., 2010) also reported the same trend, they fabricated pH-sensitive alginate/hydroxyapatite nanocomposite beads

via the in situ generation of hydroxyapatite during the sol-gel transition process of alginate. They observed that increasing the concentration of hydroxyapatite decreased the swelling capacity of the hydrogel.

3.6. Cell viability results

The viability of the cells under incubation with the hydrogels was evaluated using the MTT assay kit. The cells were incubated with the hydrogels for 24 and 72 h and the results (Fig. 8) showed that the fabricated hydrogels did not induce any adverse effect on the cells growth. Moreover, CeO₂-NPs-loaded HA hydrogels enhanced cell growth after 72 h cell seeding. These observations imply that HA hydrogel is not cytotoxic and incorporation of CeO₂-NPs improved proliferative effects of the HA hydrogels. Results of other studies are controversial, some of them showed toxicity of CeO₂-NPs and some other showed cytocompatibility. Lin et al. (Lin, 2020) reported that the synthesized CeO₂-NPs were biocompatible to chondrocytes at low concentration (lower than 0.02 μ g/mL), but at the higher concentration induce dose-dependent toxicity. Tumkur et al. (Tumkur, 2021) reported that hydroxide-mediated CeO₂-NPs did not induce cell death even at higher concentrations (100 μ g per 100 μ l), evaluated by MTT and Live/Dead assays. Arya et al. (Arya et al., 2014) reported that CeO₂-NPs not only failed to induce toxic effects on primary cortical cells, but also prevented apoptotic cell loss during treatment with hydrogen peroxide (H₂O₂, 50

μM). They suggested that the observed protective effects could be linked to the preservation or restoration of major redox equivalents, such as the NADH/NAD⁺ ratio, mitochondrial membrane potential, and cellular ATP.

3.7. Molecular evaluation result

qPCR assay was applied to reveal the regulative effects of the fabricated hydrogel on gene expressions of chondrocytes. The cells were treated with TNF- α to induce OA condition. The results (Fig. 9) showed that the expression of *Col2* and *Aggrecan* genes was downregulated under treatment with TNF- α (Control group) while expressions of *Col10*, *Mmp13*, *Adamts5*, and *Adamts9* upregulated under treatment with TNF- α (Control group), compared with healthy cells ($P < 0.05$). On the other hand, the results (Fig. 9) showed that the treatment using the hydrogel significantly reversed the effect of TNF- α (the OA condition) and restored the expression of the target genes.

ELISA results confirmed this potent antioxidant activity of hydrogel and also increased the growth of chondrocytes over the culturing period. Fig. 10 shows that concentration of *Col2*, *Aggrecan*, *Col10*, *Mmp13*, *Adamts5*, *Adamts9* in the cell culture supernatant. ELISA detected similarly a significant higher level of *Col2* and *Aggrecan* expression for treatment group compared to control (OA group), while a low level in *Col10*, *Mmp13*, *Adamts5*, *Adamts9* antigen-concentration was found in this group.

4. Conclusion

OA is an articular cartilage degenerative disease brought on by a variety of circumstances. ROS over production is widely acknowledged to be a key factor in the deterioration of articular cartilage, even if the pathophysiology of OA is still not fully understood. Potentially transformational therapeutics could result from efficient disease-modifying OA treatments. In the current assay, we combined PL and CeO₂ NPs in an injectable hydrogel fabricated from HA. We synthesized CeO₂ NPs as the antioxidant agents to modulate the overproduced ROS, the radical scavenging and antioxidant activity of CeO₂ NPs have been documented by plenty of studies. We used PL to modulate molecular pathways involved in OA. The molecular evaluations by qPCR and ELISA assays showed that the application of HA/CeO₂ NPs loaded with PL upregulated *Col2* and *Aggrecan* (TNF- α -suppressed anabolic molecules) and downregulated *Col10*, *Mmp13*, *Adamts5*, and *Adamts9* (TNF- α -activated catabolic molecules) (Yan et al., 2019). The results of the current study illustrated that the fabricated injectable HA hydrogel loaded with PL and CeO₂ NPs can be applied as the effective treatment of OA.

Declaration of competing interest

The authors declare that they have no known competing financial interests or personal relationships that could have appeared to influence the work reported in this paper.

Acknowledgement

This study was supported by the Dongguan Science and Technology of Social Development Program (grant number: 20231800935632) and Guangdong Medical Research Fund Project (grant number: A2020581).

References

Abramoff, B., Caldera, F.E., 2020. Osteoarthritis: pathology, diagnosis, and treatment options. *Med. Clin.* 104 (2), 293–311.
 Afzal, A.M., et al., 2023. Exploring the charge storage mechanism in high-performance Co@ MnO₂-based hybrid supercapacitors using Randles-Sevcik and Dunn's models. *J. Appl. Electrochem.* 1–12.

Agarwal, H., Nakara, A., Shanmugam, V.K., 2019. Anti-inflammatory mechanism of various metal and metal oxide nanoparticles synthesized using plant extracts: A review. *Biomed. Pharmacother.* 109, 2561–2572.
 Arya, A., et al., 2014. Cerium oxide nanoparticles prevent apoptosis in primary cortical culture by stabilizing mitochondrial membrane potential. *Free Radic. Res.* 48 (7), 784–793.
 Bai, Y., et al., 2019. Redox control of chondrocyte differentiation and chondrogenesis. *Free Radic. Biol. Med.* 132, 83–89.
 Celardo, L., et al., 2011. Pharmacological potential of cerium oxide nanoparticles. *Nanoscale* 3 (4), 1411–1420.
 Chen, S., et al., 2020. lncRNA Xist regulates osteoblast differentiation by sponging miR-19a-3p in aging-induced osteoporosis. *Aging Dis.* 11 (5), 1058.
 Coryell, P.R., Diekmann, B.O., Loeser, R.F., 2021. Mechanisms and therapeutic implications of cellular senescence in osteoarthritis. *Nat. Rev. Rheumatol.* 17 (1), 47–57.
 Culica, M.E., et al., 2020. Cellulose acetate incorporating organically functionalized CeO₂ NPs: efficient materials for UV filtering applications. *Materials* 13 (13), 2955.
 De Marzi, L., et al., 2013. Cytotoxicity and genotoxicity of ceria nanoparticles on different cell lines in vitro. *Int. J. Mol. Sci.* 14 (2), 3065–3077.
 Dunnick, K.M., et al., 2015. The effect of cerium oxide nanoparticle valence state on reactive oxygen species and toxicity. *Biol. Trace Elem. Res.* 166, 96–107.
 Ejaz, T., et al., 2023. Effect of Fe doping on the structural and electrochemical performance of Zn@ CuO nanostructures for energy storage device. *Solid State Ion.* 399, 116312.
 Esch, F., et al., 2005. Electron localization determines defect formation on ceria substrates. *Science* 309 (5735), 752–755.
 Farahmandjou, M., Zarinkamar, M., Firoozabadi, T., 2016. Synthesis of Cerium Oxide (CeO₂) nanoparticles using simple CO-precipitation method. *Revista Mexicana De Física* 62 (5), 496–499.
 Goldring, M.B., Otero, M., 2011. Inflammation in osteoarthritis. *Curr. Opin. Rheumatol.* 23 (5), 471.
 Hamerman, D., 1989. The biology of osteoarthritis. *N. Engl. J. Med.* 320 (20), 1322–1330.
 Hawker, G.A., King, L.K., 2022. The burden of osteoarthritis in older adults. *Clin. Geriatr. Med.* 38 (2), 181–192.
 Hezma, A., et al., 2023. Fabrication, characterization and adsorption investigation of Nano zinc oxide–sodium alginate beads for effective removal of chromium (VI) from aqueous solution. *J. Inorg. Organomet. Polym. Mater.* 33 (5), 1400–1408.
 Huang, S., et al., 2023. Targeting nano-regulator based on metal–organic frameworks for enhanced immunotherapy of bone metastatic prostate cancer. *Cancer Nanotechnol.* 14 (1), 1–15.
 Imran, M., et al., 2023. High-performance energy storage hybrid supercapacitor device based on NiCoS@ CNT@ graphene composite electrode material. *Physica Scripta* 98 (11), 115981.
 Jeuken, R.M., et al., 2016. Polymers in cartilage defect repair of the knee: current status and future prospects. *Polymers* 8 (6), 219.
 Karakoti, A., et al., 2008. Nanoceria as antioxidant: synthesis and biomedical applications. *JOM* 60, 33–37.
 Khan, R., et al., 2023. Synthesis of CNTs doped nickel copper-sulfides composite electrode material for high-performance battery-supercapacitor hybrid device. *ECS J. Solid State Sci. Technol.* 12 (10), 101005.
 Kumar, E., Selvarajan, P., Balasubramanian, K., 2010. Preparation and studies of cerium dioxide (CeO₂) nanoparticles by microwave-assisted solution method. *Recent Res. Sci. Technol.* 2 (4).
 Kwon, H.J., et al., 2016. Mitochondria-targeting ceria nanoparticles as antioxidants for Alzheimer's disease. *ACS Nano* 10 (2), 2860–2870.
 Li, L., et al., 2023. Water extracts of Polygonum Multiflorum Thunb. and its active component emodin relieves osteoarthritis by regulating cholesterol metabolism and suppressing chondrocyte inflammation. *Acupuncture Herb. Med.* 3 (2), 96–106.
 Lin, Y.-W., et al., 2020. Hyaluronic acid loaded with cerium oxide nanoparticles as antioxidant in hydrogen peroxide induced chondrocytes injury: an in vitro osteoarthritis model. *Molecules* 25 (19), 4407.
 Lu, K.H., et al., 2021. The potential remedy of melatonin on osteoarthritis. *J. Pineal Res.* 71 (3), e12762.
 Muzaffar, N., et al., 2023. Recent advances in two-dimensional metal-organic frameworks as an exotic candidate for the evaluation of redox-active sites in energy storage devices. *J. Storage Mater.* 64, 107142.
 Nelson, B.C., et al., 2016. Antioxidant cerium oxide nanoparticles in biology and medicine. *Antioxidants* 5 (2), 15.
 Nurhasanah, I., et al., 2018. Antioxidant activity and dose enhancement factor of CeO₂ nanoparticles synthesized by precipitation method. *IOP Conference Series: Materials Science and Engineering.* IOP Publishing.
 Qiu, H., et al., 2018. Inhibition of endogenous hydrogen sulfide production exacerbates the inflammatory response during urine-derived sepsis-induced kidney injury. *Exp. Ther. Med.* 16 (4), 2851–2858.
 Reed, K., et al., 2014. Exploring the properties and applications of nanoceria: is there still plenty of room at the bottom? *Environ. Sci. Nano* 1 (5), 390–405.
 Réeff, J., et al., 2013. Characterization and optimization of GMO-based gels with long term release for intraarticular administration. *Int. J. Pharm.* 451 (1–2), 95–103.
 Rhoads, J.P., Major, A.S., 2018. How oxidized low-density lipoprotein activates inflammatory responses. *Crit. Rev. Immunol.* 38 (4).
 Safat, S., et al., 2021. Enhanced sunlight photocatalytic activity and biosafety of marine-driven synthesized cerium oxide nanoparticles. *Sci. Rep.* 11 (1), 14734.
 Scanzello, C.R., Goldring, S.R., 2012. The role of synovitis in osteoarthritis pathogenesis. *Bone* 51 (2), 249–257.

- Soren, S., et al., 2015. Antioxidant potential and toxicity study of the cerium oxide nanoparticles synthesized by microwave-mediated synthesis. *Appl. Biochem. Biotechnol.* 177, 148–161.
- Sperati, A., et al., 2008. Outcomes of hip replacement: a hospital-based longitudinal study in Lazio region (Italy). *Annali Di Igiene: Medicina Preventiva e Di Comunita* 20 (2), 141–157.
- Su, S., et al., 2022. A new dressing system reduces the number of dressing changes in the primary total knee arthroplasty: A randomized controlled trial. *Front. Surg.* 9, 800850.
- Sundarrajan, P., et al., 2012. One pot synthesis and characterization of alginate stabilized semiconductor nanoparticles. *Bull. Kor. Chem. Soc.* 33 (10), 3218–3224.
- Tumkur, P.P., et al., 2021. Cerium oxide nanoparticles: Synthesis and characterization for biosafe applications. *Nanomanufacturing* 1 (3), 176–189.
- Walkey, C., et al., 2015. Catalytic properties and biomedical applications of cerium oxide nanoparticles. *Environ. Sci. Nano* 2 (1), 33–53.
- Wang, Y., et al., 2017. TLR4 rs41426344 increases susceptibility of rheumatoid arthritis (RA) and juvenile idiopathic arthritis (JIA) in a central south Chinese Han population. *Pediatr. Rheumatol.* 15, 1–8.
- Wang, Y., et al., 2023. Establishments and evaluations of post-operative adhesion animal models. *Adv. Therap.* 2200297.
- Wieland, H.A., et al., 2005. Osteoarthritis—an untreatable disease? *Nat. Rev. Drug Discov.* 4 (4), 331–344.
- Yan, L., et al., 2019. Chondroprotective effects of platelet lysate towards monoiodoacetate-induced arthritis by suppression of TNF- α -induced activation of NF- κ B pathway in chondrocytes. *Aging (Albany NY)* 11 (9), 2797.
- Zamiri, R., et al., 2015. Dielectrical properties of CeO₂ nanoparticles at different temperatures. *PLoS One* 10 (4), e0122989.
- Zhang, Y., Jordan, J.M., 2010. Epidemiology of osteoarthritis. *Clin. Geriatr. Med.* 26 (3), 355–369.
- Zhang, J., Wang, Q., Wang, A., 2010. In situ generation of sodium alginate/hydroxyapatite nanocomposite beads as drug-controlled release matrices. *Acta Biomater.* 6 (2), 445–454.
- Zhao, T., et al., 2022. Recent developments and current applications of hydrogels in osteoarthritis. *Bioengineering* 9 (4), 132.